In Situ Electrochemical Lithiation/Delithiation Observation of Individual Amorphous Si Nanorods

Hessam Ghassemi,[†] Ming Au,[‡] Ning Chen,[§] Patricia A. Heiden,[§] and Reza S. Yassar[†,*]

[†]Department of Mechanical Engineering-Engineering Mechanics, Michigan Technological University, 1400 Townsend Drive, Houghton, Michigan 49931, United States, [‡]Savannah River National Laboratory, Aiken, South Carolina 29808, United States, and [§]Department of Chemistry, Michigan Technological University, 1400 Townsend Drive, Houghton, Michigan 49931, United States

ABSTRACT *In situ* electrochemical lithiation and delithiation processes inside a nanobattery consisting of an individual amorphous Si nanorod and ionic liquid were explored. Direct formation of the crystalline $Li_{22}Si_5$ phase due to the intercalation of Li ions was observed. In addition, the role of the electrolyte—nanorod interface was examined. It was observed that the lithiation of Si nanorods is dominated by surface diffusion. Upon the delithiation process, partial decomposition of $Li_{22}Si_5$ particles was observed which can explain the irreversible capacity loss that is generally seen in Si anodes. This study shows that the radial straining due to lithiation does not cause cracking in nanorods as small in diameter as 26 nm, whereas cracks were observed during the lithiation of 55 nm Si nanorods.

KEYWORDS: lithium-ion battery · *in situ* transmission electron microscopy · nanorods · silicon · anodes

Although batteries are inherently simple in concept, surprisingly, their development has progressed much slower than other areas of electronics.[1] This slow progress is due to the lack of suitable electrode materials and electrolytes, together with difficulties in mastering the interfaces between them. Traditional lithium-ion batteries employ carbonaceous anodes with a capacity of 372 mAhg^{-1}. To obtain substantial improvement in the specific capacity of Li-ion cells, it is essential to replace carbonaceous anodes with those of greater capacity.

An attractive candidate to replace carbonaceous anodes is silicon, which has the highest theoretical capacity, in excess of 4000 mAhg^{-1} and low discharge potential upon intercalation of 4.4 Li atoms per Si atoms.[2−4] The fundamental reason behind such high capacity is that in silicon anodes each Si atom can accommodate up to 4.4 Li atoms ($Li_{22}Si_5$),[2] while in graphite, each carbon atom can accommodate 1/6 Li atom (LiC_6). A major drawback with silicon is that, upon driving Li into Si, a volume expansion of ∼300%[5,6] to 400%[7] occurs due to the formation of various phases such as $Li_{12}Si_7$, Li_7Si_3, $Li_{13}Si_4$, and $Li_{22}Si_5$.[8] This leads to induced mechanical stresses large enough to fracture and pulverize Si into powder after the first few cycles of charging/discharging and eventually loss of electrical contact and capacity fade during cycling.[4,9]

Recently, Chan *et al.*[7] studied the structural stability of Si nanowires (NW) under the lithiation/delithiation process. Despite the high capacity at the first cycle (∼4277 mAhg^{-1}), the Si NW anodes showed an irreversible capacity loss (∼1300 mAhg^{-1}) in the first charge−discharge cycle. Several scenarios may have happened, including the formation of the solid electrolyte interface (SEI) and loss of active material, the difficulty in decomposition of Li−Si phases that form during the first charging process, and the exfoliation of the active material (Li_xSi) from the electrode due to the large volume expansion caused by the alloying of Li with Si.

In theory, the one-dimensional morphology of the Si NWs was expected to improve the capacity retention of anodes due to better accommodation with lateral strains generated due to Li intercalation in the NWs. However, it is now widely known that the Si NWs have poor cyclability retention due to the fracture and pulverization of Si NWs.[4] The fracture of nanosized Si wires contradicts the previous studies that have suggested a materials-dependent terminal particle size below which particles do not fracture further.[10,11]
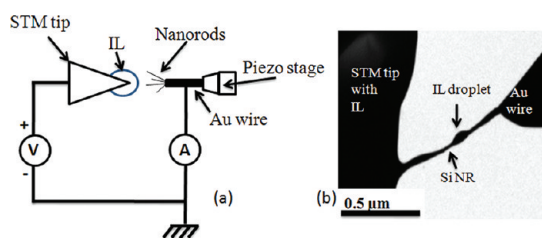
To better understand the lithiation/delithiation process in nanostructured materials, *in situ* studies of electrochemical reactions inside high-resolution electron microscopes have been proposed. Wang *et al.*[12] built a miniature prototype battery using $LiCoO_2$ as the cathode, SnO_2 nanowire

© 2011 American Chemical Society

Figure 1. (a) Schematic of STM holder experimental setup. As the STM tip is positively biased, IL flows on the nanorods and Li ions diffuse into nanorods. (b) Low-magnification image during the lithiation experiment. The arrow indicates a droplet as the IL flows on the Si NR (the other arrow) from the STM side to the gold wire.
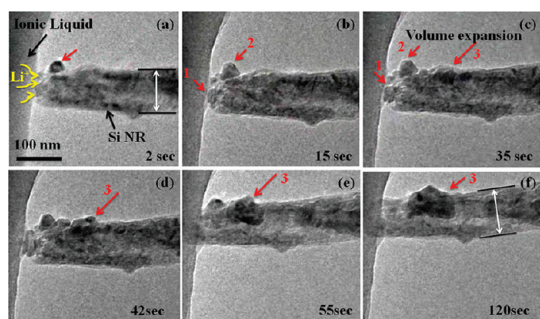
Figure 2. Snapshot series of lithiation process represents the swelling or radial straining at selective locations (indicated with red arrows) of a Si NR.

as the anode, and an ionic liquid based as the electrolyte to study the interface of Li-ion batteries inside a transmission electron microscope (TEM). Their observation provided direct imaging of the conversion of SnO_2 to Li_xSn_y and Li_zO during the charging cycle. However, due to lack of detailed study, the reaction(s) during the lithiation process, as well as the formation of phase(s), was not discussed. Briazer et al.[13] reported the first ex situ TEM observation of the cross section of a nanobattery made by stacking layers of anode and cathode to study the interface behavior, all in the solid state. Their observation indicates a rapid deterioration of the interface upon cycling due to chemical elements immigrating between the stacked layers. Recently, Huang et al.[14] reported the real time formation of the "Medusa zone", containing a high density of mobile dislocations during the lithiation of SnO_2 nanowires. The formation of this zone induced large mechanical distortion and, consequently, degradation in structural properties.

Amorphous and crystalline Si have a similar specific capacity to store Li^+; however, studies[15-17] have shown that homogeneous volume expansion in amorphous Si causes less pulverization and better cycling performance. Very recently, Huang et al.[18,19] reported the anisotropic swelling as a result of lithiation of crystalline Si NWs using in situ techniques. Formation of a dumbbell-shaped cross section led to formation of a crack in the middle of the NW along its axis. One

expects that, since there is no long-range order in the amorphous structure or preferred diffusion path, the diffusion of the same amount of Li can occur more uniformly. Here, we investigated the lithiation of individual amorphous Si nanorods using an in situ electrochemical setup inside the TEM technique. Two different diffusion paths, longitudinal and radial, were examined, and the formation of Li_xSi phases was confirmed by diffraction pattern studies that agree with our ex situ lithiation results.

RESULTS

Selective Lithiation of Si NRs. Figure 1a depicts the in situ lithiation setup where a drop of IL is placed on the STM tip and individual Si NRs are placed on the gold wire. Then by the help of piezo-driven stage, the gold wire is moved toward the STM tip until an individual Si NR is in contact with the IL (Figure 1a). The applied bias voltage, in range of 3−4 V, introduces surface tension to the IL stream on the NR, which causes Plateau−Rayleigh instability phenomenon[20] and breaks the stream into droplets, as shown in Figure 1b.

Figure 2 shows still images of an in situ video showing the effect of lithiation on the geometrical structure of Si nanorods. The yellow arrows indicate the main diffusion path for Li^+ into the NR, as that is the contact point between the NR and ILs. The red arrows in Figure 2 indicate the preferential locations where significant volume straining was observed. In Figure 2a, the ionic liquids containing Li ions are located on the far left side of the image, and the Si NR was brought into contact with ILs. In less than 2 s, the first changes were observed on the tip of NR (location 1) and an area very close to the tip (location 2), as shown by the red arrows. These areas of the NR continued to grow and became larger in size; however, their growth was almost stopped after 14 s and another area (location 3) started to expand in volume (Figure 2c). This location of the nanorod continued to grow, as shown by the red arrows in Figure 2c−f. Also, the radial straining is marked on Figure 2a,f and measured to be almost 10%. The volume expansion in Si during lithiation is due to the formation of Li_xSi phases.[2,7,14]

Overall, two important observations can be made here. First, the lithiation process does not start only at the contact point where the IL and NR meet. The process rather starts at selective areas close to the surface of the NR. This is somewhat in contrast with the recent observation of the lithiation process in crystalline SnO_2 nanowires where the lithiation process was propagated into the nanowire from the interface.[14] In principle, due to surface coverage of ionic liquids on the nanorod, the surface diffusion, which has lower activation energy compared to that of bulk, can be a faster path for the Li ions to be transferred to the
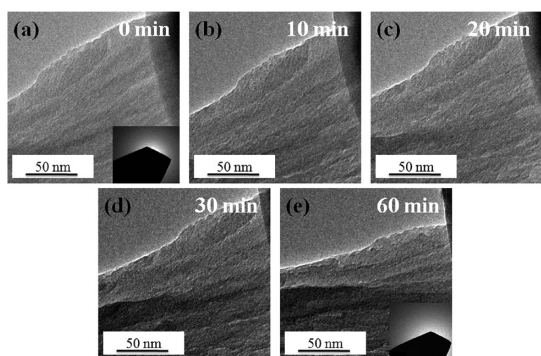
Figure 3. Amorphous Si NR in contact with the IL that has no Li content at (a) 0 min, (b) 10 min, (c) 20 min, (d) 30 min, (e) 60 min. Insets in (a) and (e) show the diffraction pattern of the Si NR initially and after 1 h of experiment.

nanorods. In this scenario, the Li ions will face larger barrier energy to diffuse into bulk Si in comparison to the surface channels.[21,22] It is shown by Gai et al.[23] that, due to the reduced energy barriers in nanomaterials, formation of the $Li_{12}Si_7$ phase takes place at lower temperature and applied voltage compared to that of the bulk Si structure.

Second, there is selectiveness to the lithiation locations within the nanorod. Initially, locations 1 and 2 became lithiated and then location 3 grew. While it is unclear why the lithiation is localized in particular areas, speculations can be made on the presence of structural disorder within the Si nanorods. The switching from locations 1 or 2 to location 3 can be explained by the fact that, upon lithiation and associated nanoscale crack formation during volume straining, the diffusion path for Li ions will be disconnected. The interruption in Li channels will result in the stoppage of volume growth and consequently the lithiation of other locations.

In order to identify if the observed structural features are due to the insertion of lithium into the NR, a number of experiments were conducted with the same IL but with no lithium content. Figure 3a shows an amorphous Si NR that is in contact with the IL. It can be seen that, after 60 min of being in contact with ILs with no Li content (Figure 3e), no detectable deformation and/or phase formation was observed. The diffraction pattern shown in the insets of Figure 3a,e also indicates that the structure of the Si NR remained amorphous after 60 min. Therefore, the formations of particles observed in Figure 2 are due to the diffusion of the Li into the Si NR and consequently the formation of Li_xSi phases.

***In Situ/Ex Situ* Phase Transformation during Lithiation.** In order to understand if the phase transformations observed during the lithiation of Si NRs were assisted by the electron beam radiation, the structure of the *in situ* lithiated nanorods was compared with the ones lithiated *ex situ*. The *ex situ* experiments were conducted in a half-cell where a beaker cell of Li-ion
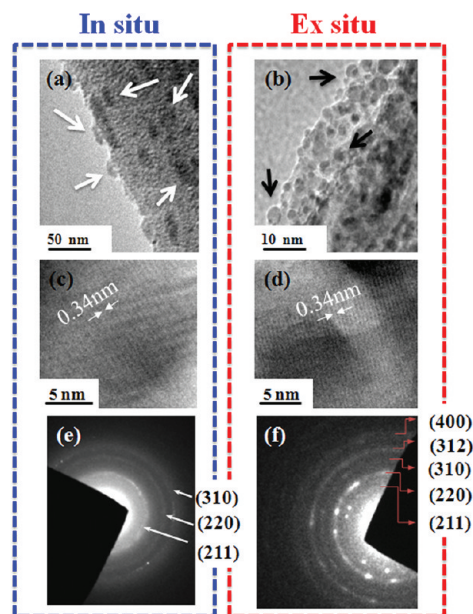

Figure 4. (a) *In situ* charged Si NR contains several particles of $Li_{22}Si_5$ phase marked by white arrows. Similar particle morphology was observed in the *ex situ* fully charged Si NRs as shown in (b). (c,d) HRTEM images of the $Li_{22}Si_5$ particles indicating the crystalline nature of the lithiated phase. The *d* spacing as shown in (d) measured to be 0.34 nm. (e,f) Electron diffraction patterns of the lithiated NRs in *in situ* and *ex situ* experiments, respectively.

battery was constructed in a VAC (vacuum atmosphere cooperation) glovebox filled with argon gas. Both the Si NR array sample and a Li foil (Aldrich) were inserted in the cell as the anode and cathode. The 1 M $LiPF_6$ in PC/DMC (propylene carbonate and dimethyl carbonate) was used as the electrolyte. Princeton Applied Physics' VersaSTAT-3 was used for the measurement of electrochemical properties of the anodes. The galvanic charge—discharge was carried out at 700 mA/g from 0.01 to 3.00 V.

Figure 4 compares the high-resolution TEM images and diffraction patterns of an *in situ* lithiated nanorod and an *ex situ* lithiated nanorod. In Figure 4a,b, the bright-field TEM images of *in situ* and *ex situ* lithiated nanorods are shown in low magnifications. Both nanorods have similar distribution of dark contrast particles. These particles formed during the charging cycle and are expected to be various forms of Li_xSi phases. Interestingly, these particles are crystalline, which means that amorphous Si transforms to crystalline Li_xSi during lithiation. Figure 4c,d shows HRTEM images of the $Li_{22}Si_5$ particles. The *d* spacing was measured to be 0.34 nm in the *in situ* lithiated sample, which is in good agreement with that of the *ex situ* lithiated samples and other reported results.[24] Due to the crystallinity of these phases and associated strain energy of their formation, one expects these particles to be darker in comparison to the surrounding amorphous matrix. The analysis of the diffraction patterns shown in the Figures 4e,f indicates that these Li_xSi particles are in
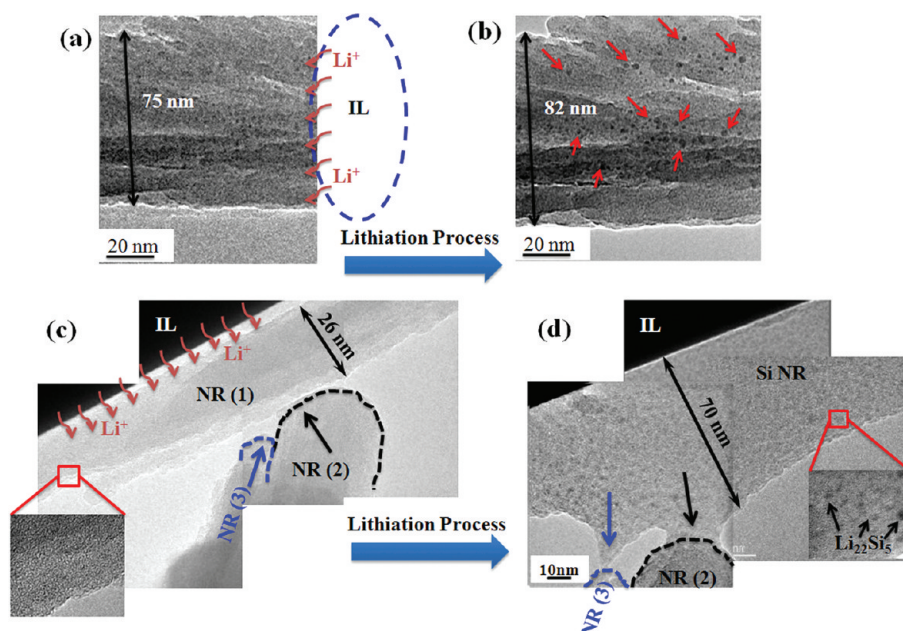
Figure 5. (a) Individual Si NR that is in contact with the IL before lithiation. The Li-ion diffusion is along the axis of the nanorod. Image in (b) shows the NR after lithiation process with straining of ~10% in diameter. (c) Individual Si NR in contact with IL from the side surface. The thickness of the NR was measured to be 26 nm before the lithiation and high-resolution image (inset) shows the amorphous structure of NR before lithiation. (d) After the lithiation process, the diameter of NR expanded to 70 nm. Inset shows a high-resolution image of $Li_{22}Si_5$ particles formed as a result of lithiation.

fact $Li_{22}Si_5$ phases. This study indicates that the *in situ* lithiation experiments in TEM are in complete agreement with the *ex situ* charging tests, and therefore, the electron-beam-assisted modification of Li-ion diffusion can be ruled out. In addition, one should note that the phase identification in this study has been mainly based on HRTEM and diffraction analysis. In future research, it will be interesting to study the possibility for the existence of any Li_xSi amorphous phases using electron energy loss spectroscopy (EELS).

According to the Li–Si phase diagram,[25] various forms of Li–Si alloys can form including LiSi, $Li_{12}Si_7$, and $Li_{22}Si_5$. One expects the formation of a series of the Li_xSi_y phases as the concentration of Li increases in the Si structure. However, in this study, we only observed the direct formation of the $Li_{22}Si_5$ phase inside the amorphous Si. This is in contrast with the X-ray diffraction (XRD) results of Obrovac et al.[26] and Hatchard et al.,[27] where $Li_{15}Si_4$ was identified to be the fully lithiated phase during the lithiation of Si at room temperature.

This apparent discrepancy can be explained from both thermodynamic and kinetic points of view. The standard Gibbs free energy for $Li_{22}Si_5$ is calculated to be −273 kcal/mol as opposed to that of $Li_{12}Si_7$ which is −199 kcal/mol.[28] Hence, from the thermodynamic point of view, the direct formation of crystalline $Li_{22}Si_5$ is expected to be more favorable than amorphous silicon. One should also note that the structure of Si nanorods is amorphous, meaning that no long-range order in atomic arrangements exists. This disordering in the structure of amorphous Si can act as diffusion

channels for the Li ions to transport faster the crystalline Si.[29] Therefore, from the kinetic point of view, there is higher tendency to form the fully lithiated (and the most stable) form of Li–Si alloy. Measurements by Wilkening et al.[29] also indicated that activation energy of amorphous $LiNbO_3$ is less than 1/3 of the microcrystalline one. Therefore, diffusivity of elements such as Li in amorphous structures is much higher than that of the nanocrystal and microcrystal ones. The last point is that the results from both Obrovac et al.[26] and Hatchard et al.[27] showed that there was a critical thickness of 2 μm above which the crystalline $Li_{15}Si_4$ could form. In the case of NRs, since the diffusion path for the Li atoms is significantly lower than that of the above-mentioned thick layers of a-Si, each Si atom can be surrounded by higher number of Li, resulting in the formation of $Li_{22}Si_5$. Experimental results from another group also confirmed the formation of $Li_{22}Si_5$ phase, and 4200 mAhg^{-1} storage capacity was reported.[7]

Effect of Contact Area in Ionic Liquid–Nanorod Interfaces. Figure 5 depicts the *in situ* lithiation process for the two different cases where Si NRs and ILs are in contact with each other. In Figure 5a, the tip of a Si NR is in contact with IL (the Li$^+$ path is shown schematically), and the lithiated Si NR is shown in Figure 5b. As discussed before, the formation of $Li_{22}Si_5$ phases was observed (marked by arrows). The overall radial straining of this NR was measured to be ~10%. Figure 5c shows an individual NR where the sides of the NR are in contact with IL. In order to better show the structural changes, three TEM images were overlaid. The sides of the NR (1) are in contact with IL, and the NR (2) and NR (3) were

used to designate the region where the radial straining was observed (Figure 5c). The initial diameter of NR (1) was measured to be ~26 nm, and its amorphous structure is shown in the inset of Figure 6c. Similar to the case in Figure 5b, the formation of $Li_{22}Si_5$ phase was observed as indicated by arrows in the inset of Figure 5d. The NR (1) expanded from 26 to 70 nm as a result of Li insertion that can be estimated to be close to 270% straining in a radial direction. Note, our intention is mainly to capture the swelling of the NRs rather than the total volume straining. Therefore, we did not keep track of the longitudinal straining of the NRs as they perhaps elongate into the ILs.

Inside a conventional Li-ion battery, anodes and cathodes are actually immersed into the electrolyte. However, in the case where only the tip of NRs was in contact with the ILs (Figure 6a), the regions of the NR close to the IL source were exposed to a higher Li
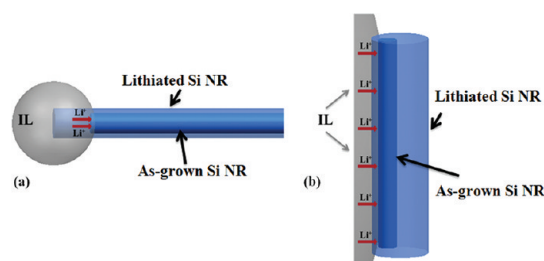
density compared to the areas away from the NR. This can also explain why the majority of lithiation activities in Figure 2 were observed in areas close to ILs. In the case where the side of Si NRs is immersed into ILs (Figure 6b), Li ions have a larger surface area to diffuse into the NR. Therefore, one expects the NR to expand more in order to accommodate the volumetric strains. Therefore, increasing the surface area with an electrolyte in Si NRs in ILs can better mimic the real condition of battery charging.

In Situ Delithiation Process. By reversing the applied bias on the lithiated NR, the discharging process can be studied. A nanorod was lithiated inside TEM, as shown in Figure 7I-a−I-c, and 15% straining in diameter was measured. By comparing Figure 7II-a−II-c, one can see that the density of small particles was increased as a result of decomposition of larger particles upon delithiation. Also, the *in situ* delithiated NRs show 10% shrinkage in overall diameter as a result of Li deintercalation. The shrinkage in diameter is due to the decomposition of $Li_{22}Si_5$ to the structures with smaller unit cell volume (for instance $Li_{12}Si_7$ in ref 30) or full extraction of Li ions from $Li_{22}Si_5$ phase. In fact, the white arrows in Figure 7II-a and II-c point out a particle that is completely vanished during delithiation. In addition, in comparison to the initial diameter (Figure 7I-a), the delithiated NR (Figure 7II-c) has a larger diameter by 5%. This residual straining means that some of the Li ions that intercalated into Si did not leave the Si structure upon delithiation. This conclusion also explains the irreversible capacity loss that has been observed in Si structures.[4,7]
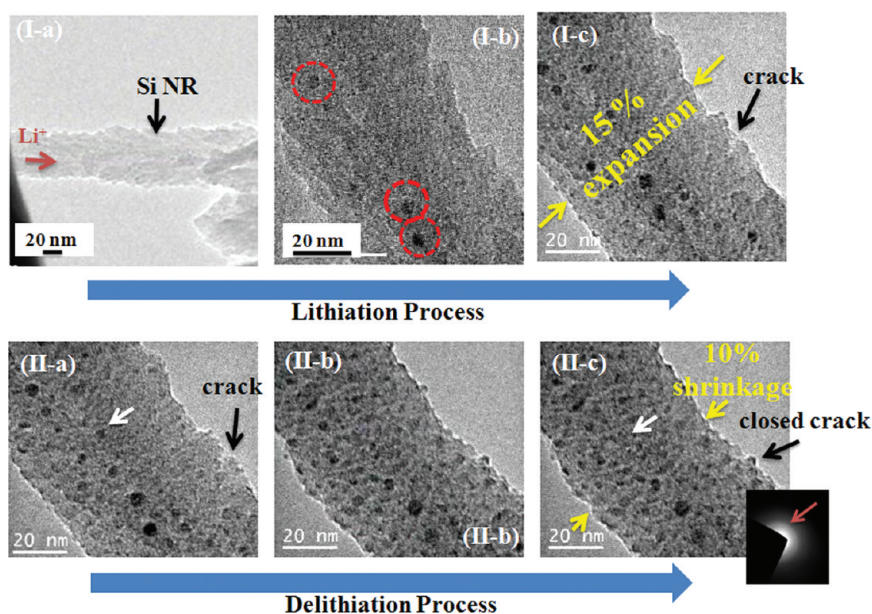

Figure 6. Schematics of two cases of interactions at IL−NR interfaces are shown. Schematic (a) illustrates the case where IL is in contact with the tip of a Si NR. Schematic (b) represents a case where the sides of NR are dipped into the IL.

Figure 7. (I-a−I-c) *In situ* lithiation of an individual Si nanorod. Images on (I-b) and (I-c) represent the formation of $Li_{22}Si_5$ after 20 and 30 min, respectively. The arrow in image I-c indicates a crack formed on the surface of Si NR during lithiation process. (II-a−II-c) Delithiation process is shown. The white arrow in image II-a points to a $Li_{22}Si_5$ particle that disappears during the delithiation process, as shown in II-b and II-c. In addition, a crack closure can be seen by comparing the images II-a and II-c and tracking the black arrow.

It is generally speculated that the reduction of size in silicon to nanometer range should improve its fracture toughness during lithiation.[10,31,32] However, mechanical failure in the form of crack formation was observed in our lithiated NRs. This means that the induced mechanical stresses due to lithiation can be large enough to initiate cracks and eventually to pulverize nanoscale silicon into particles. Huggins and Nix[10] calculated the critical size for fracture of a particle subjected to lithiation as below:

$$h_c = \frac{23}{\pi}\left(\frac{3k_{Ic}}{B\varepsilon_T}\right)^2$$

where h_c is the critical size, K_{Ic} is the fracture roughness in MPa$\sqrt{m}$, B is the biaxial Young's modulus of the material, and ε_T is the total strain. For silicon, the fracture toughness is 10 MPa$\sqrt{m}$, and the strain due to formation of $Li_{22}Si_5$ is $\approx$400%.[7] Therefore, the critical size under which the fracture does not happen can be estimated to be 75 nm. Here, the cracks were detected in the 55 nm Si NRs (marked by a dark arrow in Figure 7II-a), which contradicts the theoretical predictions given in ref 10. In our case, Si NRs with diameters less than 26 nm did not show crack formation upon lithiation (Figure 5d). This means that the theoretical models should be corrected in order to predict the true critical size scale below which one should not expect cracking in Si upon lithiation. However, it should be kept in mind that deterministic conclusion on an exact size scale will be too speculative at this stage due to lack of statistical analysis.

CONCLUSION

In summary, one life cycle of the lithiation/delithiation process on a nanobattery was performed using an *in situ* electrochemical setup inside a transmission electron microscope. Direct formations of $Li_{22}Si_5$ particles were recorded. Our results show that the NRs are subjected to higher radial straining when there is larger surface area for the diffusion of Li ions into the Si nanorods. The results suggest that there is a size-scale regime beyond which the fracture toughness of Si nanorods is larger than the strain energy required to induce cracking in Si nanorods. The Si nanorods with diameters of 26 nm did not fracture upon lithiation, while nanorods with 55 nm were cracked. In addition, $Li_{22}Si_5$ particles were not fully decomposed when subjected to delithiation. This observation can explain the irreversible capacity loss in Si structures used in Li-ion battery technologies.

EXPERIMENTAL PROCEDURE

The pure Si nanorods were fabricated by an oblique angle (co)deposition technique in a custom-designed two-source electron-beam deposition system, where two quartz crystal microbalances (QCMs) were installed to monitor the near-normal deposition thickness and rate of each source independently.[33]

Individual Si NRs were then attached to a gold wire by light mechanical scratching on the as-grown samples. As a result of van der Waals forces, individual NRs stick to the wire in different directions. The piezo-driven holder allows nanometer motion of the sample toward the AFM tip. Sample position can be adjusted with a precision of 1 nm in *X*, *Y*, and *Z* directions. High-resolution TEM images and electron diffraction patterns were collected to characterize the formation of different phases during the lithiation of different individual Si NRs.

Supporting Information Available: HRTEM images of the as-grown Si NRs, XRD results of the as-grown and 100 cycle lithiated samples, experimental procedure of ionic liquid synthesis. This material is available free of charge *via* the Internet at http://pubs.acs.org.

Note Added after ASAP Publication: This paper originally published ASAP on September 20, 2011. The Acknowledgment section was updated and the revised version was reposted on September 29, 2011.

REFERENCES AND NOTES

1. Armand, M.; Tarascon, J.-M. Building Better Batteries. *Nature* **2008**, *451*, 652–657.
2. Boukamp, B. A.; Lesh, G. C.; Huggins, R. A. All-Solid Lithium Electrodes with Mixed-Conductor Matrix. *J. Electrochem. Soc.* **1981**, *128*, 725–729.
3. Green, M.; Fielder, E.; Scrosati, B.; Wachtler, M.; Moreno, J. S. Structured Silicon Anodes for Lithium Battery Applications. *Electrochem. Solid-State Lett.* **2003**, *6*, A75–A79.
4. Kasavajjula, U.; Wang, C.; Appleby, A. J. Nano- and Bulk-Silicon-Based Insertion Anodes for Lithium-Ion Secondary Cells. *J. Power Sources* **2007**, *163*, 1003–1039.
5. Baggetto, L.; Niessen, R. A. H.; Roozeboom, F.; Notten, P. H. L. High Energy Density All-Solid-State Batteries: A Challenging Concept towards 3D Integration. *Adv. Funct. Mater.* **2008**, *18*, 1057–1066.
6. Yang, J.; Winter, M.; Besenhard, J. O. Small Particle Size Multiphase Li-Alloy Anodes for Lithium-Ion-Batteries. *Solid State Ionics* **1996**, *90*, 281–287.
7. Chan, C. K.; Peng, H.; Liu, G.; McIlwrath, K.; Zhang, X. F.; Huggins, R. A.; Cui, Y. High-Performance Lithium Battery Anodes Using Silicon Nanowires. *Nat. Nanotechnol.* **2008**, *3*, 31–35.
8. Föll, H.; Hartz, H.; Ossei-Wusu, E.; Carstensen, J.; Riemenschneider, O. Si Nanowire Arrays as Anodes in Li Ion Batteries. *Phys. Status Solidi RRL* **2010**, *4*, 4–6.
9. Maranchi, J. P.; Hepps, A. F.; Evans, A. G.; Nuhfer, N. T.; Kumta, P. N. Interfacial Properties of the a-Si/Cu:Active− Inactive Thin-Film Anode System for Lithium-Ion Batteries. *J. Electrochem. Soc.* **2006**, *6*, A1246–A1253.
10. Huggins, R. A.; Nix, W. D. Decreptiation Model for Capacity Loss during Cycling of Alloys in Rechargeable Electrochemical Systems. *Ionics* **2000**, *6*, 57–63.
11. Yang, J.; Winter, M.; Besenhard, J. O. Small Particle Size Multiphase Li-Alloy Anodes for Lithium-Ion-Batteries. *Solid State Ionics* **1996**, *90*, 281–287.

12. Wang, C. M.; Xu, W.; Liu, J.; Choi, D. W.; Arey, B.; Saraf, L. V.; Zhang, J. G.; Yang, Z. G.; Thevuthasan, S.; Baer, D. R.; *et al. In-Situ* Transmission Electron Microscopy and Spectroscopy Studies of Interfaces in Li Ion Batteries: Challenges and Opportunities. *J. Mater. Res.* **2010**, *25*, 1541–1547.

13. Brazier, A.; Dupont, L.; Dantras-Laffont, L.; Kuwata, N.; Kawamura, J.; Tarascon, J.-M. First Cross-Section Observation of an All Solid-State Lithium-Ion "Nanobattery" by Transmission Electron Microscopy. *Chem. Mater.* **2008**, *20*, 2352–2359.

14. Huang, J. Y.; Zhong, L.; Wang, C. M.; Sullivan, J. P.; Xu, W.; Zhang, L. Q.; Mao, S. X.; Hudak, N. S.; Liu, X. H.; Subramanian, A.; *et al. In Situ* Observation of the Electrochemical Lithiation of a Single SnO_2 Nanowire Electrode. *Science* **2010**, *330*, 1515–1520.

15. Beaulieu, L. Y.; Eberman, K. W.; Turner, R. L.; Krause, L. J.; Dahn, J. R. Colossal Reversible Volume Changes in Lithium Alloys. *Electrochem. Solid-State Lett.* **2001**, *4*, A137–A140.

16. Yin, J. T.; Wada, M.; Yamamoto, K.; Kitano, Y.; Tanase, S.; Sakai, T. Micrometer-Scale Amorphous Si Thin-Film Electrodes Fabricated by Electron-Beam Deposition for Li Ion Batteries. *J. Electrochem. Soc.* **2006**, *153*, A472–A477.

17. Maranchi, J. P.; Hepp, A. F.; Kumta, P. N. High Capacity, Reversible Silicon Thin-Film Anodes for Lithium-Ion Batteries. *Electrochem. Solid-State Lett.* **2003**, *6*, A198–A201.

18. Liu, X. H.; Zheng, H.; Zhong, L.; Huang, S.; Karki, K.; Zhang., L. Q.; Liu, Y.; Kushima, A.; Liang, W. T.; Wang, J. W.; *et al.* Anisotropic Swelling and Fracture of Silicon Nanowires during Lithiation. *Nano Lett.* **2011**, *11*, 3312–3318.

19. Liu, X. H.; Zhang, L. Q.; Zhong, L.; Liu, Y.; Zheng, H.; Wang, J. W.; Cho, J. H.; Dayeh, S. A; Picraux, S. T.; Sullivan, J. P.; *et al.* Ultrafast Electrochemical Lithiation of Individual Si Nanowire Anodes. *Nano Lett.* **2011**, *11*, 2251–2258.

20. Brochard-Wyard, F.; De Gennes, P. Quere, D. *Capillarity and Wetting Phenomena: Drops, Bubbles, Pearls, Waves*; Springer: Berlin; ISBN 0-387-00592-7.

21. Hofmann, S.; Csanyi, G.; Ferrari, A. C.; Payne, M. C.; Robertson, J. Surface Diffusion: The Low Activation Energy Path for Nanotube Growth. *Phys. Rev. Lett.* **2005**, *95*, 036101–036104.

22. Tanemura, M.; Iwata, K.; Takahashi, K.; Fujimoto, Y.; Okuyama, F.; Sugie, H.; Filip, V. Growth of Aligned Carbon Nanotubes by Plasma-Enhanced Chemical Vapor Deposition: Optimization of Growth Parameters. *J. Appl. Phys.* **2001**, *90*, 1529–1533.

23. Gai., B.; Saion, S.; Fleming, L.; Zhou, O. Alloy Formation in Nanostructured Silicon. *Adv. Mater.* **2003**, *13*, 816–819.

24. Zhou, Y. N.; Li, W. J.; Chen, H. J.; Liu, C.; Zhang, L.; Fu, Z. Nanostructured NiSi Thin Flms as a New Anode Material for Lithium Ion Batteries. *Electrochem. Commun.* **2011**, *13*, 546–549.

25. Okamoto, H. The Li—Si (Lithium—Silicon) System. *Binary Alloy Phase Diagram* **1990**, *11*, 306–312.

26. Obrovac, M. N.; Christensen, L. Structural Changes in Silicon Anodes during Lithium Insertion/Extraction. *Electrochem. Solid-State Lett.* **2004**, *7*, A93–A96.

27. Hatchard, T. D.; Dahn, J. R. *In Situ* XRD and Electrochemical Study of the Reaction of Lithium with Amorphous Silicon. *J. Electrochem. Soc.* **2004**, *151*, A838–A842.

28. Anani, A. A.; Huggins, R. A. Kinetic and Thermodynamic Parameters of Several Binary Lithium Alloy Negative Electrode Materials at Ambient Temperature. *J. Electrochem. Soc.* **1987**, *134*, C407.

29. Wilkening, M.; Bork, D.; Indris, S.; Heitjans, P. Diffusion in Amorphous $LiNbO_3$ Studied by ^7Li NMR—Comparison with the Nano- and Microcrystalline Material. *Phys. Chem. Chem. Phys.* **2002**, *4*, 3246–3251.

30. Kang, K.; Lee, H. S.; Han, D. W.; Kim, G. S.; Lee, D.; Lee, G.; Kang, Y. M.; Jo, M. H. Maximum Li Storage in Si Nanowires for the High Capacity Three Dimensional Li-Ion Battery. *Appl. Phys. Lett.* **2010**, *96*, 053110–053113.

31. Dimov, N.; Kugino, S.; Yoshio, M. Mixed Silicon—Graphite Composites as Anode Material for Lithium Ion Batteries Influence of Preparation Conditions on the Properties of the Material. *J. Power Sources* **2004**, *136*, 108–114.

32. Aifantis, K. E.; Dempsey, J. P. Stable Crack Growth in Nanostructured Li-Batteries. *J. Power Sources* **2005**, *143*, 203–211.

33. He, Y. P.; Zhang, Z. Y.; Hoffmann, C.; Zhao, Y. P. Embedding Ag Nano Particles into MgF_2 Nanorod Arrays. *Adv. Funct. Mater.* **2008**, *18*, 1676–1684.